Mission Profile Based Adaptive Carrier Frequency Control for Modular Multilevel Converters for Medium Voltage Applications

Wang, Zhongxu; Wang, Huai; Zhang, Yi; Blaabjerg, Frede

Published in:
Proceedings of 2019 10th International Conference on Power Electronics and ECCE Asia (ICPE 2019 - ECCE Asia)

Publication date:
2019

Document Version
Accepted author manuscript, peer reviewed version

Mission Profile Based Adaptive Carrier Frequency Control for Modular Multilevel Converters for Medium Voltage Applications

Zhongxu Wang, Huai Wang, Yi Zhang, Frede Blaabjerg
Department of Energy Technology, *Aalborg University*, Aalborg, Denmark
zho@et.aau.dk, hwa@et.aau.dk, yiz@et.aau.dk, fbl@et.aau.dk

***Abstract*—In order to increase the efficiency and to improve the reliability of modular multilevel converters in medium voltage applications, this paper proposes an adaptive control method to choose an optimal carrier frequency dynamically according to power loading conditions of the modular multilevel converter. By evaluating the impact of the carrier frequency on the output current harmonic performance and the capacitor voltage ripple analytically, the proposed adaptive control can reduce the power loss and the thermal stress on the power semiconductors. Meanwhile, the electrical operation requirements can still be fulfilled. One-year mission profile is utilized to assess the energy efficiency and the reliability performance between the proposed and the traditional control scheme. Moreover, theoretical analyses and simulation results are presented to demonstrate the effectiveness of the proposed control.**

I. Introduction

Modular Multilevel Converters (MMCs) are promising candidates for medium-voltage applications, such as wind power generation [1] and medium-voltage motor drives [2]. The MMC can easily be extended to high voltage levels by increasing the number of Sub-Modules (SMs). Correspondingly, its current level, system power loss, and cost of energy under the same power loading condition decreases.

However, due to the variable power loading, especially in wind power generation applications, power semiconductors in the MMCs are exposed to severe thermal stress that is critical to its reliability performance. A series of studies have been conducted to evaluate the thermal stress of the MMCs under different operation conditions [3]–[7], and it can be found that severe thermal imbalance exists among power devices in the SMs. In order to balance the thermal loading among devices and to improve the reliability of the MMC, several approaches are proposed in the prior-art by optimizing the power loss distribution and conducting active thermal control. The impact of several available control freedoms in the MMC, including the circulating current and dc voltage offset on the power loss are evaluated, and simulation results show their negligible contribution to the loss reduction. The multi-objective optimization control proposed in [8] concludes that the decrease of the capacitor voltage can reduce the switching loss, and a similar idea is proposed and validated experimentally in [9]. However, this method is valid for MMCs with a low or medium number of SMs only. By combining the temperature balancing with the capacitor voltage balancing control, the thermal imbalance among SMs are relieved and the lifetime is improved according to simulations [10] and experiments [11]. However, the energy efficiency is not fully analyzed, which is always a big concern for the active thermal control. As a matter of fact, the conduction loss is mainly dominated by the arm current and is independent of the modulation techniques for the MMCs [12]. There is a little room for the loss and thermal stress reduction regarding the conduction loss. Thus, more attention should be paid to the switching loss reduction. Minimizing the switching frequency is a straightforward way to achieve this objective. A flexible switching frequency control proposed in [13] can reduce the junction temperature fluctuations by changing the switching frequency in wind power converters. However, no mathematical analysis is given to guide the selection of the carrier frequency.

In this paper, a mission profile based adaptive carrier frequency control is proposed for MMCs for medium voltage applications. The impact of the carrier frequency on the operation of the MMC is evaluated analytically in order to fulfill its operation requirements. Moreover, the energy efficiency based on mission profile is calculated for comparison with the traditional control method.

II. Adaptive Carrier Frequency Control for Modular Multilevel Converters

For MMCs utilized in medium voltage applications, the number of SM per arm is not large and Phase-Shifted Carrier (PSC) modulation is commonly used [14]. The basic concept of the proposed adaptive carrier frequency control is to change the carrier frequency of the PSC dynamically according to the power loading over a wide range of the input power. In practical applications for the MMC applied in the grid integration, the adaptive control is able to achieve a higher system efficiency by exploring the minimum carrier frequency under certain requirements. Meanwhile, the reliability of the whole MMC system can be improved due to the improved thermal stress of the power semiconductors. Thus, the key is how to choose the carrier frequency in terms of the requirements for the output current and the SM capacitor voltage ripple. In the following, the impacts of the carrier frequency on the output current harmonics and the capacitor voltage ripple are analyzed respectively.

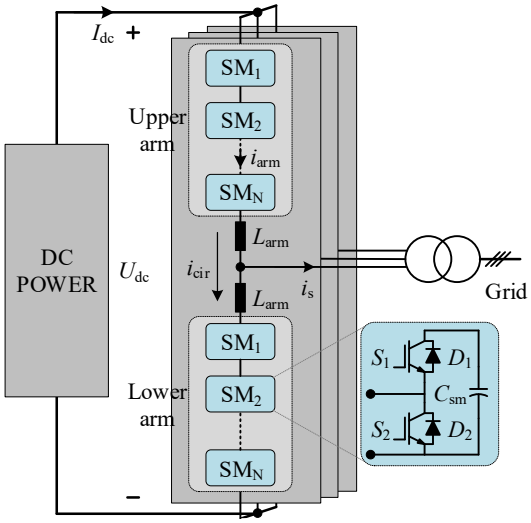

Fig. 1. Typical three-phase MMC system. (i_{cir} is the circulating current, L_{arm} is the arm inductance, i_{s} is the output current, i_{arm} is the arm current, U_{dc} is the DC bus voltage, i_{dc} is the DC current and C_{sm} is the SM capacitance.)

A. Impact of Carrier Frequency on Output Current Harmonic

According to the MMC model in [15], the output current is driven by the output voltage of the MMC, which is the difference between the lower arm voltage and the upper arm voltage. Thus, in order to explore the impact of the carrier frequency on the output current, the double Fourier series analysis has to be applied to obtain all harmonic components in the SM output voltage. By summing up all SM voltages, the converter output voltage u_s can be obtained as

$$\begin{cases} u_{\mathrm{s}} = \dfrac{1}{2}\left(u_{\mathrm{n}} - u_{\mathrm{p}}\right) = H(u_{\mathrm{s}})_{\mathrm{f}} \cdot \cos\left(\omega_1 t\right) + H(u_{\mathrm{s}})_{a,b} \\ \qquad \times \cos\left(\left(Na\omega_{\mathrm{c}} + b\omega_1\right)t + \dfrac{Na\theta + b\pi - \pi}{2}\right) \\ H(u_{\mathrm{s}})_{\mathrm{f}} = \dfrac{mU_{\mathrm{dc}}}{2} \\ H(u_{\mathrm{s}})_{a,b} = \dfrac{2U_{\mathrm{dc}}}{a\pi N} \sin\left[\dfrac{\left(Na+b\right)\pi}{2}\right] \\ \qquad \times J_b\left(\dfrac{mNa\pi}{2}\right) \cos\left(\dfrac{Na\theta + b\pi - \pi}{2}\right) \end{cases} \tag{1}$$

where $u_{\mathrm{p/n}}$ is the upper and lower arm voltage; J_b is the Bessel function of the first kind; ω_{c} is the angular frequency of carrier; θ is the angular displacement between the carriers of upper and lower arms. N is the SM number per arm; $H(u_{\mathrm{s}})_{\mathrm{f}}$ and $H(u_{\mathrm{s}})_{a,b}$ are the amplitude of the fundamental and harmonic component of output voltage.

If an ideal grid condition without harmonics is assumed, the harmonics in the output current will only be driven by the harmonics in the output voltage u_{s}. As for the fundamental component of the output current, it is driven by the power loading condition. Thus, the Total Harmonic Distortion (THD) of the output current is expressed as

$$\begin{cases} THD\left(i_{\mathrm{s}}\right) = \dfrac{\sqrt{\sum_{a=1}^{\infty}\sum_{b=-\infty}^{\infty} H\left(i_{\mathrm{s}}\right)_{a,b}^2}}{H(i_{\mathrm{s}})_f} \\ H(i_{\mathrm{s}})_{\mathrm{f}} = \dfrac{2P}{3H(u_{\mathrm{s}})_f \cos\left(\varphi\right)} \\ H(i_{\mathrm{s}})_{a,b} = \dfrac{H(u_{\mathrm{s}})_{a,b}}{\left(Na\omega_{\mathrm{c}} + b\omega_1\right)\left(L_{\mathrm{arm}}/2\right)} \end{cases} \tag{2}$$

where P is the power loading; $H(i_{\mathrm{s}})_{\mathrm{f}}$ and $H(i_{\mathrm{s}})_{a,b}$ are the amplitude of the fundamental and harmonic component of the output current, and φ is the power factor angle; L_{arm} is the arm inductance in the MMC.

TABLE I
MAIN SYSTEM PARAMETERS FOR THE CASE STUDY.

Power rating P	15 MVA	DC link voltage U_{dc}	20 kV
SM number per arm N	8	Arm inductance L_{arm}	4.1 mH
SM voltage U_{sm}	2.5 kV	SM capacitance C_{sm}	3.0 mF
Modulation index m	0.9	Case temperature T_{c}	40 °C

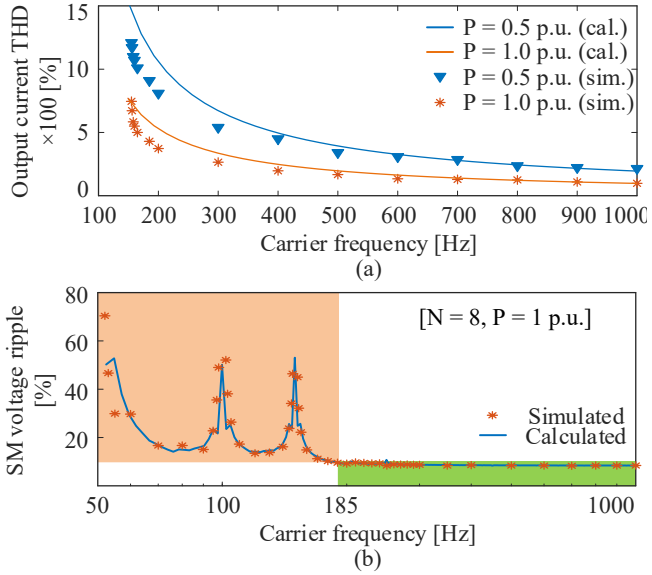

Fig. 2. Impact of the carrier frequency on the output current THD and the capacitor voltage ripple. (a) Simulated and calculated output current THD under two power loadings; (b) Simulated and calculated capacitor voltage ripple under unity power loading.

Fig. 2(a) shows the simulated and calculated output current THD under two power loading conditions. It can be seen that the calculated results agree well with the simulations in the high carrier frequency range, and error increases in the low carrier frequency range, especially between 150 Hz and 300 Hz. This is caused by the omission of the harmonics in the arm reference and the capacitor voltage ripple.

B. Impact of Carrier Frequency on SM Voltage Ripple

The impact of the carrier frequency on the capacitor voltage ripple needs to be evaluated, especially when the carrier frequency is as low as several times the fundamental frequency. The capacitor voltage can be obtained by conducting integration of the capacitor current, which is defined by the arm current and the switching sequence. To simplify the analysis, harmonics in the circulating current and the output current are ignored. Considering the negligible impact of the angular displacement of the carriers on the voltage ripple, only one SM capacitor voltage of phase A is taken as an example, and can be mathematically evaluated by

$$\begin{cases} u_{\mathrm{sm,p}} = U_{\mathrm{sm}} + \\ \dfrac{1}{C_{\mathrm{sm}}} \displaystyle\int \left[\left(\begin{array}{l} \frac{1}{2} - \frac{m}{2}\cos(\omega_1 t) + \\ K_{a,b}\cos(a\omega_{\mathrm{c}} t + b\omega_1 t + b\pi) \end{array} \right) \left(i_{\mathrm{cir}} + \frac{1}{2} i_{\mathrm{s}} \right) \right] \\ K_{a,b} = \displaystyle\sum_{a=1}^{\infty} \sum_{b=-\infty}^{\infty} \frac{2}{a\pi} \sin\left[\frac{(a+b)\,\pi}{2} \right] \times J_b\left(\frac{ma\pi}{2} \right) \end{cases} \tag{3}$$

where $u_{\mathrm{sm,p}}$ and U_{sm} are the instantaneous voltage and the average voltage across the capacitor; C_{sm} is the submodule capacitance; i_{cir} is the circulating current.

Fig. 2(b) shows the simulated and the calculated capacitor voltage ripple under unity power loading. The calculated voltage ripple values agree well with the simulation results. It means the omission of the harmonics in the current is reasonable, and (3) can be used for further analysis in the following. It can also be seen that integer carrier frequency of the fundamental frequency can cause the divergence of the capacitor voltage which should be avoided. Besides that, the voltage ripple almost keeps constant when the carrier frequency is higher than a specific threshold (e.g., 185 Hz for a maximum of 10% voltage ripple).

C. Proposed Adaptive Carrier Frequency Control

Based on the above analysis, the carrier frequency boundary for a specific output current THD and capacitor voltage ripple requirement (e.g., THD of the output current is less than 5%, and the voltage ripple is less than 10% of the average voltage) can be obtained as shown in Fig. 3. The main MMC system parameters listed in Table I as a case study. The dotted green and blue lines refer to the carrier frequency-power loading operating boundary of this MMC system in order to limit to 5% THD of the output current for two different carrier angular displacements, respectively. For the fixed carrier frequency control, the minimum carrier frequency is 440 Hz to fulfill all the above requirements by setting the angular displacement $\theta = \pi/8$. Note that, in this case, the circulating current harmonic performance becomes the worst. On the contrary, the best harmonic performance of the circulating current can be achieved when the angular displacement is $\theta = 0$, and the harmonic performance of the output current will be the worst.

In addition, in order to meet the capacitor voltage ripple requirement and to avoid the main integer carrier frequencies

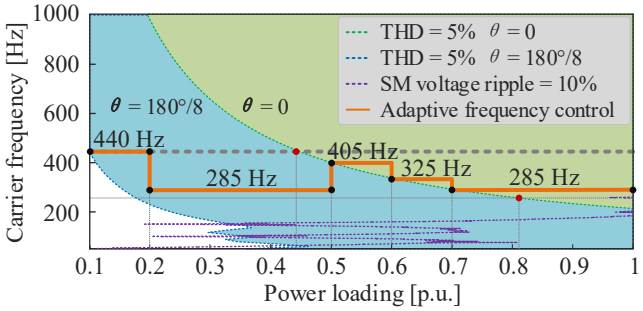

Fig. 3. Carrier frequency selection strategy according to the power loading, the output current THD, and the capacitor voltage ripple.

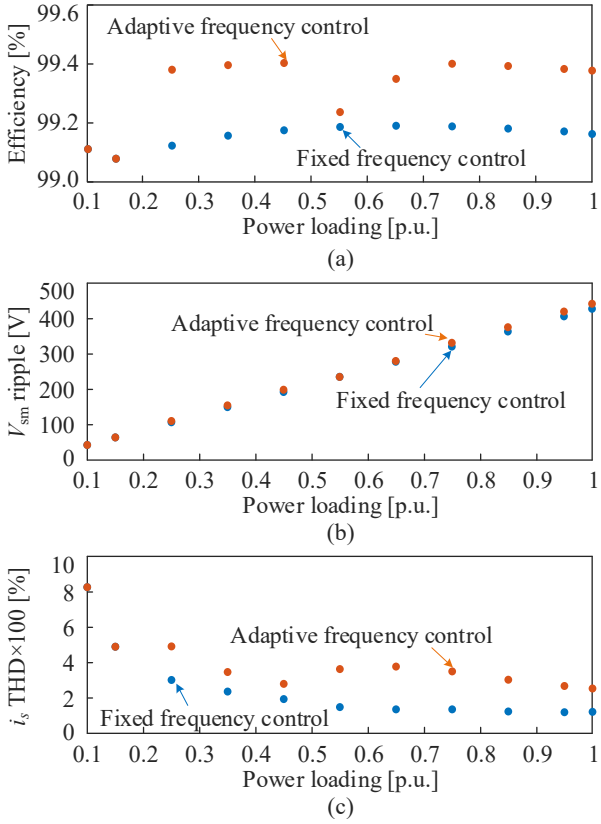

Fig. 4. Simulation results of the system efficiency, the capacitor voltage ripple, and the output current THD under different power loading conditions.

(e.g., 100 Hz, 150 Hz, 200 Hz, and 250 Hz), the carrier frequency is chosen higher than 250 Hz. For an easy and practical implementation, discrete carrier frequencies determined by predefined power loading intervals (e.g., 10% power loading change) are used in this paper. The final carrier frequency implementation strategy is thus according to the orange line shown in Fig. 3 to achieve the lowest possible switching frequency of the MMC. Note that, in order to ensure the harmonic performance of the circulating current, $\theta = 0$ is applied first for the power loading higher than 0.5 p.u., and $\theta = \pi/8$ is applied for the power loading lower than 0.5 p.u..

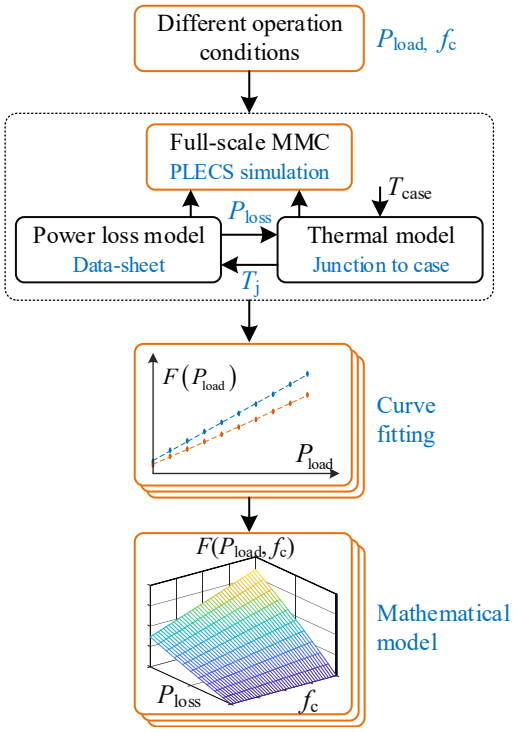

Fig. 5. Mission profile translation to the power loss profile and the thermal loading profile.

Based on the MMC system listed in Table I, the operating performances of the proposed adaptive frequency control and fixed frequency control are compared under different power loading conditions. It can be seen from Fig. 4(a) that the system efficiency is improved by around 0.2% with the proposed control method under most power loading ranges. Meanwhile, the SM capacitor voltage ripple is still within 10% limit, namely 500 V. In addition, the output current harmonic performance deteriorates due to the decrease of the carrier frequency. However, the THD keeps below 5% in most of the power loading range (e.g., higher than 0.2 p.u.).

III. Mission Profile Translation to Power Loss and Thermal Stress Profiles

In order to validate the proposed adaptive frequency control, practical operating condition, namely a mission profile, is taken into account to evaluate the performance difference between the two different control strategies. As a case study, a MMC applied in wind power generation is considered with a power rating of 15 MVA considering five 3-MVA wind turbines. A one-year wind speed profile with a resolution of 10 minutes/data is analyzed. A mission profile based multi-disciplinary analysis method aiming for a long-term simulation is utilized in [16]. Its evaluation process is depicted in Fig. 5. Instead of conducting the real-time simulation based on one-year mission profile, several discrete operating conditions (e.g., different power loadings and carrier frequencies) are simulated based on the full-scale three-phase MMC, where the power loss model and the thermal model of the devices are

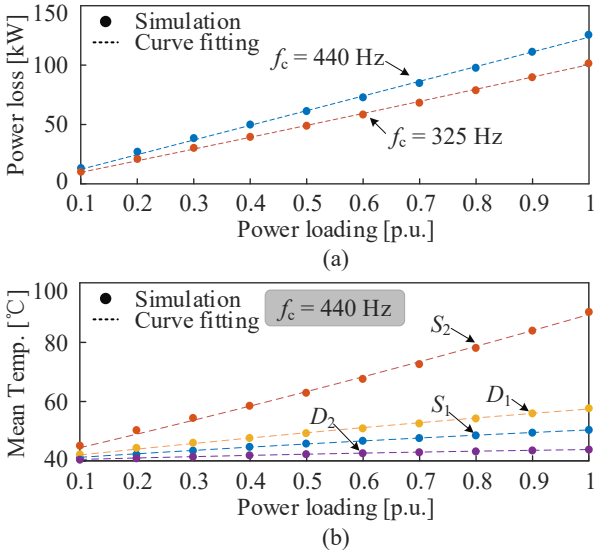

Fig. 6. Impact of the power loading on the system power loss and the mean junction temperature.

obtained from the data-sheet [17]. Afterwards, the relationship between the parameters of interest (e.g., the system power loss, the mean junction temperature and the junction temperature cycle amplitude of the power devices) and different operating conditions (e.g., the power loading and the carrier frequency) can be established by curve fitting and is depicted through mathematical models.

Fig. 6 shows the impact of the power loading on the system power loss with the carrier frequency being 325 Hz and 440 Hz and the mean junction temperature amplitude of the four power devices in a half-bridge SM. Their relationship can be well curve fitted by a second-order polynomial. Similarly, as shown in Fig. 7, the impact of the carrier frequency can be curve fitted by a one-order polynomial as

$$\begin{cases} F\left(P_{\text{load}}\right) = a_1 P_{\text{load}}^2 + a_2 P_{\text{load}} + a_3 \\ F\left(f_c\right) = a_4 f_c + a_5, \end{cases} \tag{4}$$

where $F(x)$ refers to the junction temperature cycle amplitude ΔT, the mean junction temperature T_{m}, and the system power loss P_{loss}; x refers to the power loading P_{load} and the carrier frequency f_c (Note that the power loading is normalized ranging from 0 to 1); a_i $(i = 1...5)$ are constants obtained from the curve fitting.

Since $F(x)$ shows a proportional relationship with the carrier frequency in the range of 250 - 650 Hz, which covers the carrier frequency used in the proposed adaptive frequency control, a mathematical model describing the relationship between $F(x)$, the power loading, and carrier frequency is

$$\begin{aligned} F\left(P_{\text{load}}, f_c\right) = & \frac{F(P_{\text{load}})_{@440\text{Hz}} - F(P_{\text{load}})_{@325\text{Hz}}}{440 - 325} \\ & \times (f_c - 325) + F(P_{\text{load}})_{@325\text{Hz}} \end{aligned}, \tag{5}$$

where $F(P_{\text{load}})_{@325\text{Hz}}$ and $F(P_{\text{load}})_{@440\text{Hz}}$ are the curve-fitted polynomial under the carrier frequency of 325 Hz and

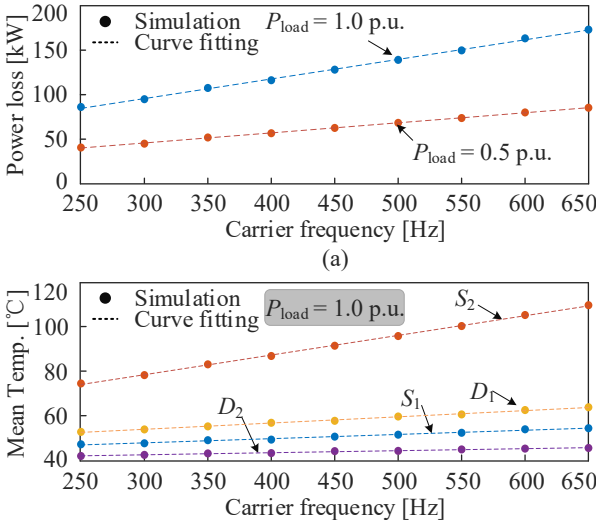

Fig. 7. Impact of the carrier frequency on the system power loss and the mean junction temperature.

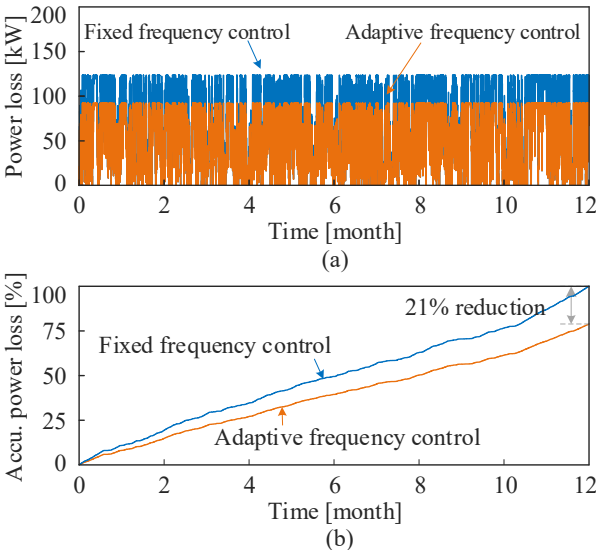

Fig. 8. Impact of the carrier frequency on the system power loss and the mean junction temperature.

440 Hz, respectively.

By establishing this 3-D model, the mission profile can easily be translated into the power loss and thermal stress profiles. The system power loss with different control approaches are shown in Fig. 8(a) and 21% annual power loss reduction of the IGBT power modules can be achieved as seen in Fig. 8(b) by applying the adaptive frequency control, which means a 0.188% yearly energy efficiency increase. It can be seen from Figs. 9(a) and 9(b) that the amplitude decrease of the highest junction temperature cycle amplitude and the mean junction temperature amplitude are about 2.3 °C and 12.4 °C, respectively. The reduced thermal stress will contribute to an improved reliability and a longer lifetime of the power devices.

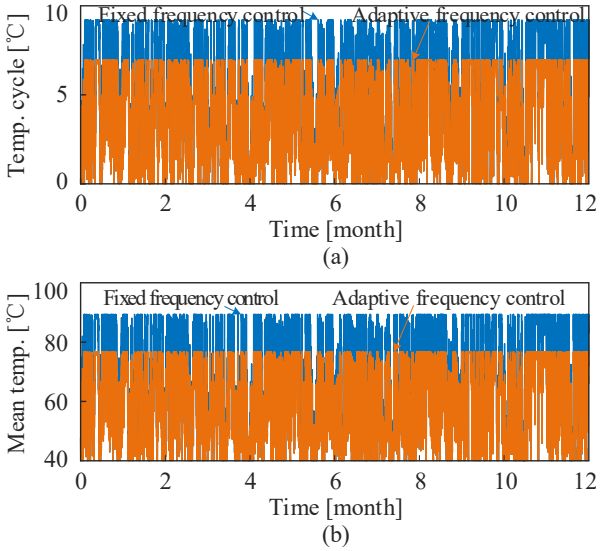

Fig. 9. Impact of the carrier frequency on the system power loss and the mean junction temperature.

IV. Reliability Evaluation of the Proposed Adaptive Frequency Control

A. Reliability Evaluation

Temperature and temperature variation are one of the key stressors induce degradation of the IGBT modules [18]. Therefore, a thermal cycle counting algorithm needs to be applied to obtain the thermal stress information. The most commonly used method is Rainflow counting [19], [20]. Fig. 10 shows the rainflow counting results of the most stressed power devices in one SM with the two control methods. It can be seen that both the cycle average and the cycle amplitude are reduced by applying the adaptive frequency control.

In order to analyze the accumulated effect of the varying stress conditions, Miner's rule [21] is used by assuming that the impact of different thermal stresses on the damage is independent on the time it happens. Thus, the impact of repetitive thermal stresses on the power semiconductors can be evaluated by an empirical lifetime model developed from accelerated testing [22] as

$$N_f = A(\Delta T_{\mathrm{j}})^{\alpha} \cdot \exp\left(\frac{E_a}{k_b T_{\mathrm{jm}}}\right), \tag{6}$$

where N_f is the number of cycles to failure under particular stress condition. $A = 3.025 \times 10^5$, $\alpha = -5.039$, $E_a = 9.891 \times 10^{-20}$J, and k_b is the Boltzmann constant; ΔT_{j} and T_{jm} are the junction temperature variation and the mean junction temperature in unite of Kelvin.

As it can be expected, taking the most stressed power component S_2 for example, the reduced thermal stress resulting from the adaptive frequency control will cause less damage during the annual mission profile. As shown in Fig. 11, the annually accumulated damage is reduced by 12% with the adaptive frequency control. Accordingly, the MMC system expects to have a longer lifetime than the case with the fixed

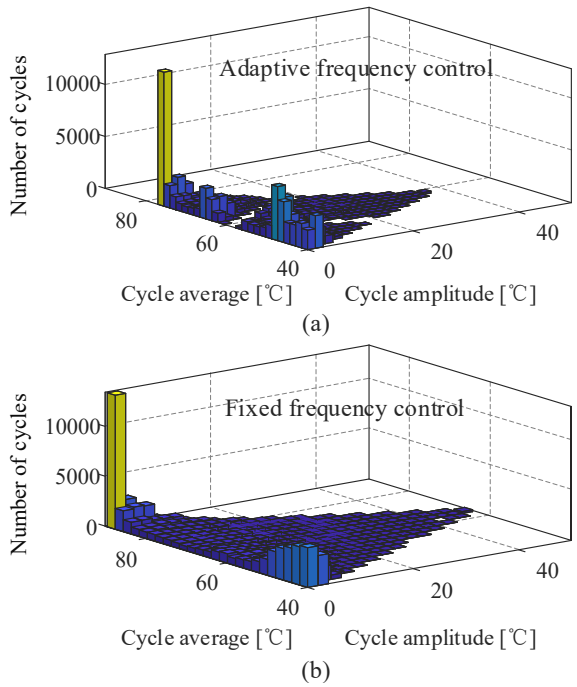

Fig. 10. Rainflow counting results of the most stressed power device S_2 with the adaptive and the fixed frequency control during one year of operation.

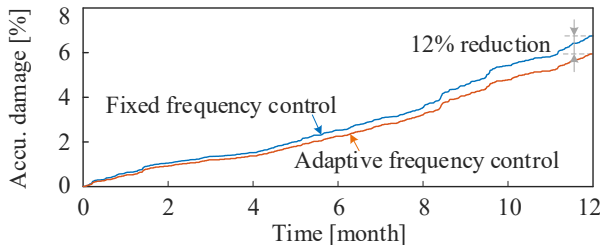

Fig. 11. Accumulated damage of the most stressed power device S_2 with the adaptive and the fixed frequency control during one year of operation.

frequency control. It means less maintenance requirement and reduced operation cost.

V. Conclusion

A mission-profile based adaptive carrier frequency control is proposed to increase the energy efficiency and to improve the reliability performance of the MMC. The impacts of the carrier frequency on the output current THD and the capacitor voltage ripple are evaluated to obtain its boundary regarding different power loading conditions. A series of optimized carrier frequencies are chosen according to the power loading conditions. Simulation results have shown 0.19% annual efficiency gain and reduced thermal stress of the IGBT modules. The accumulated damage of the most stressed IGBT device decreases by 12% compared with fixed frequency control.

References

[1] X. Yuan, "A set of multilevel modular medium-voltage high power converters for 10-MW wind turbines," *IEEE Trans. Sustain. Energy*, vol. 5, no. 2, pp. 524–534, 2014.

[2] A. Marzoughi, R. Burgos, D. Boroyevich, and Y. Xue, "Design and Comparison of Cascaded H-Bridge, Modular Multilevel Converter, and 5-L Active Neutral Point Clamped Topologies for Motor Drive Applications," *IEEE Trans. Ind. Appl.*, vol. 54, no. 2, pp. 1404–1413, 2018.

[3] M. Andresen, K. Ma, G. De Carne, G. Buticchi, F. Blaabjerg, and M. Liserre, "Thermal Stress Analysis of Medium-Voltage Converters for Smart Transformers," *IEEE Trans. Power Electron.*, vol. 32, no. 6, pp. 4753–4765, 2017.

[4] H. Liu, K. Ma, and F. Blaabjerg, "Device loading and efficiency of modular multilevel converter under various modulation strategies," in *Proc. IEEE 7th Int. Symp. Power Electron. Distrib. Gener. Syst.*, Jun. 2016, pp. 1–7.

[5] K. Li, Z. Zhao, L. Yuan, S. Lu, and G. Feng, "An improved phase-shifted carrier-based modulation and loss distribution analysis for MMC using full bridge sub-modules," in *Proc. IEEE 8th Int. Power Electron. Motion Control Conf.*, Jul. 2016, pp. 1252–1258.

[6] P. D. Judge and T. C. Green, "Dynamic thermal rating of a Modular Multilevel Converter HVDC link with overload capacity," in *Proc. IEEE Eindhoven PowerTech, PowerTech*, Sep. 2015, pp. 1–6.

[7] X. Han, Q. Yang, L. Wu, and M. Saeedifard, "Analysis of thermal cycling stress on semiconductor devices of the Modular Multilevel Converter for drive applications," in *Proc. IEEE Appl. Power Electron. Conf. Expo.*, May 2016, pp. 2957–2962.

[8] Q. Yang and M. Saeedifard, "Active thermal loading control of the modular multilevel converter by a multi-objective optimization method," in *Proc. IEEE Annual Conf. Ind. Electron. Society*, Oct. 2017, pp. 4482–4487.

[9] J. Goncalves, D. J. Rogers, and J. Liang, "Submodule Temperature Regulation and Balancing in Modular Multilevel Converters," *IEEE Trans. Ind. Electron.*, vol. 65, no. 9, pp. 7085–7094, 2018.

[10] A. Sangwongwanich, L. Mathe, R. Teodorescu, C. Lascu, and L. Harnefors, "Two-dimension sorting and selection algorithm featuring thermal balancing control for modular multilevel converters," in *Proc. IEEE 18th European Conf. Power Electron. Appl.*, Sep. 2016, pp. 1–10.

[11] F. Hahn, M. Andresen, G. Buticchi, and M. Liserre, "Thermal analysis and balancing for modular multilevel converters in hvdc applications," *IEEE Trans. Power Electron.*, vol. 33, no. 3, pp. 1985–1996, Mar. 2018.

[12] Z. Wang, H. Wang, Y. Zhang, and F. Blaabjerg, "Balanced conduction loss distribution among sms in modular multilevel converters,," in *Proc. IEEE Inter. Power Electron. Conf.*, Otc. 2018, pp. 3123–3128.

[13] Z. Qin, H. Wang, F. Blaabjerg, and P. C. Loh, "The feasibility study on thermal loading control of wind power converters with a flexible switching frequency," in *Proc. IEEE Energy Convers. Congr. Expo.*, Otc. 2015, pp. 485–491.

[14] B. Li, R. Yang, D. Xu, G. Wang, W. Wang, and D. Xu, "Analysis of the phase-shifted carrier modulation for modular multilevel converters," *IEEE Trans. Power Electron.*, vol. 30, no. 1, pp. 297–310, 2015.

[15] K. Sharifabadi, L. Harnefors, H. P. Nee, S. Norrga, and R. Teodorescu, *Design, control and application of modular multilevel converters for HVDC transmission systems*, 2016, no. United Kingdom: Wiley.

[16] Y. Yang, H. Wang, F. Blaabjerg, and K. Ma, "Mission profile based multi-disciplinary analysis of power modules in single-phase transformerless photovoltaic inverters," in *Proc. 15th Eur. Conf. Power Electron. Appl.*, Otc. 2013, pp. 1–10.

[17] ABB, "IGBT Module 5SNA 1200G450350," in *Data-sheet*, Mar. 2016.

[18] M. S. Haque, S. Choi, and J. Baek, "Auxiliary particle filtering-based estimation of remaining useful life of IGBT," *IEEE Trans. Ind. Electron.*, vol. 65, no. 3, pp. 2693–2703, 2018.

[19] M. Musallam and C. M. Johnson, "An efficient implementation of the rainflow counting algorithm for life consumption estimation," *IEEE Trans. Reliab.*, vol. 61, no. 4, pp. 978–986, 2012.

[20] L. R. GopiReddy, L. M. Tolbert, B. Ozpineci, and J. O. Pinto, "Rainflow Algorithm-Based Lifetime Estimation of Power Semiconductors in Utility Applications," *IEEE Trans. Ind. Appl.*, vol. 51, no. 4, pp. 3368–3375, 2015.

[21] M. A. Miner, "Cumulative damage in fatigue," *J. Appl. Mech. Trans. ASME*, vol. 12, no. 4, p. A159A164, 1945.

[22] R. Bayerer, T. Herrmann, T. Licht, J. Lutz, and M. Feller, "Model for power cycling lifetime of IGBT modules - various factors influencing lifetime," *Proc. 5th Int. Conf. Integr. Power Syst.*, pp. 1–6, Jun. 2011.